

## Origin of orbital ordering in $\text{YTiO}_3$ and $\text{LaTiO}_3$

Xue-Jing Zhang, Erik Koch, and Eva Pavarini

*Institute for Advanced Simulation, Forschungszentrum Jülich, 52425 Jülich, Germany*



(Received 14 April 2020; accepted 15 June 2020; published 6 July 2020)

The origin of orbital order in correlated transition-metal compounds is strongly debated. For the paradigmatic  $e_g$  systems  $\text{KCuF}_3$  and  $\text{LaMnO}_3$ , it has been shown that the electronic Kugel'-Khomskii mechanism alone is not sufficient to drive the orbital-ordering transition up to the high temperatures at which it is experimentally observed. In the case of  $t_{2g}$  compounds, however, the role played by the superexchange interaction remains unclear. Here we investigate this question for two representative systems, the  $3d t_{2g}^1$  Mott insulators  $\text{LaTiO}_3$  and  $\text{YTiO}_3$ . We show that the Kugel'-Khomskii superexchange transition temperature  $T_{\text{KK}}$  is unexpectedly large, comparable to the value for the  $e_g^3$  fluoride  $\text{KCuF}_3$ . By deriving the general form of the orbital superexchange Hamiltonian for the  $t_{2g}^1$  configuration, we show that the  $\text{GdFeO}_3$ -type distortion plays a key part in enhancing  $T_{\text{KK}}$  to about 300 K. Still, orbital ordering above 300 K can be ascribed only to the presence of a static crystal-field splitting.

DOI: [10.1103/PhysRevB.102.035113](https://doi.org/10.1103/PhysRevB.102.035113)

### I. INTRODUCTION

Orbital order in strongly correlated materials can arise from different types of microscopic mechanisms [1]. The first is the classical Jahn-Teller instability; in this scenario, the electron-lattice coupling produces lattice distortions which remove the orbital degeneracy. The crystal-field splitting arising via such distortions can lead to large differences in orbital occupations and regular patterns of mostly occupied orbitals, i.e., to orbital ordering. Remarkably, even if the crystal-field splitting is relatively small in comparison to the bandwidth, the orbital polarization can be large since it is strongly enhanced by the Coulomb interaction [2–4], making orbital ordering stable even at very high temperatures. The second mechanism that can lead to orbital ordering phenomena is the electronic superexchange introduced by Kugel' and Khomskii [5]. In this mechanism the ordering arises even in the absence of crystal-field splitting and is due to the orbital superexchange interaction. The strength of such a purely electronic mechanism has been investigated in detail for the case of the paradigmatic  $e_g$  systems  $\text{KCuF}_3$  and  $\text{LaMnO}_3$ . It has been shown that the associated transition temperature  $T_{\text{KK}}$  is too small to explain the presence of orbital ordering well above 1000 K [4,6–8], as observed experimentally. In the case of  $\text{KCuF}_3$  it was shown that even the electron-phonon coupling alone does not explain experimental findings; instead, a new mechanism was identified in which the Born-Mayer repulsion plays a key role [9]. This new mechanism is particularly relevant for ionic systems. Finally, for layered perovskites yet another mechanism, the orbital superexchange field, was shown to be at work in addition [10].

In this complex scenario, it remains to be established how strong superexchange effects are in  $t_{2g}$  materials. Representative systems are the  $3d t_{2g}^1$  orthorhombic perovskites  $\text{LaTiO}_3$  and  $\text{YTiO}_3$ , two strongly correlated insulators with  $\text{GdFeO}_3$ -type structure (see Fig. 1) [12,13]. Both compounds are paramagnetic insulators in a wide temperature range. For

$\text{YTiO}_3$  the magnetic transition temperature to the ferromagnetic ground state is as low as 40 K. Orbital ordering has been detected via various experimental techniques ranging from nuclear magnetic resonance [14] to polarized neutron diffraction [15,16], x-ray magnetic diffraction [17], the joint refinement method [18], resonant x-ray scattering [19], and soft x-ray linear dichroism [20]. For  $\text{LaTiO}_3$  the situation is more complex. In  $t_{2g}$  perovskites the gain in superexchange energy from static Jahn-Teller orbital ordering is expected to be much smaller than in  $e_g$  systems, where orbitals are bond oriented. It was therefore suggested that in  $\text{LaTiO}_3$  the proximity to the metal-insulator transition could make the (dynamical) orbital liquid state stable instead [21]. Later, however, evidence in favor of orbital ordering accumulated, as it became clear that, although the Jahn-Teller distortion is very small, a sizable static crystal-field splitting is generated by the  $\text{GdFeO}_3$ -type distortion and the associated deformations of the cubic cation cage [2,3,22–28]. While it is now accepted that  $\text{LaTiO}_3$  is orbitally ordered, it still remains to be established what role the superexchange interaction actually plays in the genesis of such ordering, which, for  $\text{LaTiO}_3$  as for  $\text{YTiO}_3$ , persists well above the magnetic ordering temperature. This is what we investigate and clarify in this work.

This paper is organized as follows. In Sec. II we describe the model and method used. The technique we adopt is based on the dynamical mean-field theory (DMFT). It is augmented with the approach we established in Ref. [4] for studying superexchange-driven orbital-ordering transitions. In Sec. III we present the main results. We calculate the order parameter, the orbital polarization  $p(T)$ , as a function of temperature. We obtain the transition temperature  $T_{\text{KK}}$ , which marks the onset of the orbitally ordered phase for the pure superexchange mechanism, and identify the most occupied natural orbital. We show that in both  $\text{LaTiO}_3$  and  $\text{YTiO}_3$  the critical temperature  $T_{\text{KK}}$  is surprisingly large with respect to some early assumptions. We find  $T_{\text{KK}} \sim 300$  K, comparable

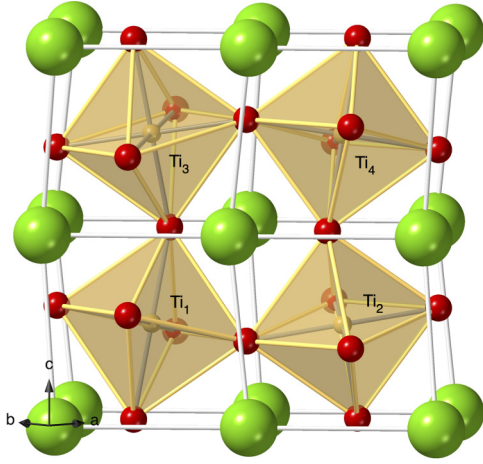


FIG. 1. The GdFeO<sub>3</sub>-type perovskite structure [11] of LaTiO<sub>3</sub>. The pseudocubic axes are  $\mathbf{x} \sim (\mathbf{a} + \mathbf{b})/2$ ,  $\mathbf{y} \sim (\mathbf{b} - \mathbf{a})/2$ ,  $\mathbf{z} \sim \mathbf{c}$ . Point symmetry transformations with respect to site Ti<sub>1</sub> are  $(\hat{x} \leftrightarrow \hat{y})$  for site Ti<sub>2</sub>,  $(\hat{z} \leftrightarrow -\hat{z})$  for site Ti<sub>3</sub>, and  $(\hat{x} \leftrightarrow \hat{y}), (\hat{z} \leftrightarrow -\hat{z})$  for site Ti<sub>4</sub>.

to the case of the  $e_g^3$  perovskite KCuF<sub>3</sub>. We show that this is mostly due to the GdFeO<sub>3</sub>-type distortion. Remarkably, our results show that the superexchange interaction alone favors a very similar orbital ordering in YTiO<sub>3</sub> and LaTiO<sub>3</sub>. There is, however, an important difference between the two compounds. In YTiO<sub>3</sub>, where the GdFeO<sub>3</sub>-like distortion is larger, the superexchange interaction cooperates with the static crystal-field splitting in determining the orbital which is actually occupied; the most occupied natural orbital obtained without crystal-field splitting is very close to the one obtained in the presence of the static crystal-field splitting and observed experimentally. In contrast, for LaTiO<sub>3</sub>, a system with a much smaller GdFeO<sub>3</sub>-like distortion, it substantially differs; that is, the superexchange interaction partially competes with the static crystal-field splitting. The conclusions are summarized in Sec. IV. In the Appendix we present the general orbital superexchange Hamiltonian for the  $t_{2g}^1$  configuration, used in the discussion presented in Sec. III.

## II. MODEL AND METHOD

In the first step we perform local density approximation (LDA) calculations using the full-potential linearized augmented plane-wave method as implemented in the WIEN2K code [29]. The LDA bands are shown in Fig. 2. Next, we construct localized  $t_{2g}$ -like Wannier functions using projectors and, when needed, the maximal localization procedure [30]. The Wannier orbitals obtained in this way for the experimental structures are shown in Fig. 3. Finally, we build the associated  $t_{2g}$  Hubbard model with full local Coulomb interaction

$$\begin{aligned} \hat{H} = & - \sum_{ii'} \sum_{\sigma} \sum_{mm'} t_{mm'}^{i,i'} c_{im\sigma}^\dagger c_{im'\sigma} + U \sum_{im} \hat{n}_{im\uparrow} \hat{n}_{im\downarrow} \\ & + \frac{1}{2} \sum_{i\sigma\sigma'} \sum_{m \neq m'} (U - 2J - J\delta_{\sigma,\sigma'}) \hat{n}_{im\sigma} \hat{n}_{im'\sigma'} \\ & - J \sum_{im \neq m'} (c_{im\uparrow}^\dagger c_{im\downarrow}^\dagger c_{im'\uparrow} c_{im'\downarrow} + c_{im\uparrow}^\dagger c_{im\downarrow} c_{im'\downarrow}^\dagger c_{im'\uparrow}). \quad (1) \end{aligned}$$

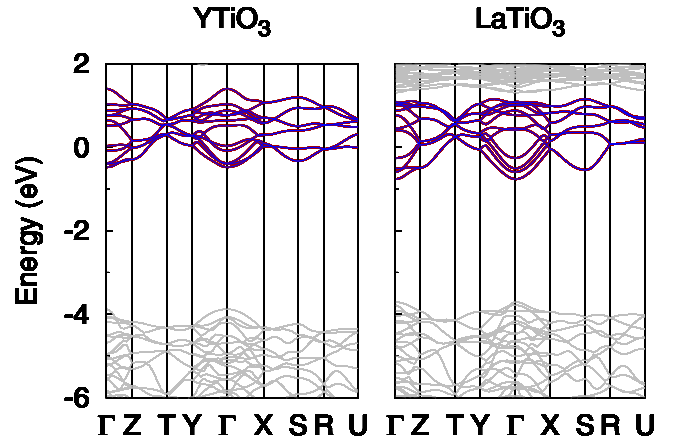


FIG. 2. Light gray: LDA band structure of YTiO<sub>3</sub> (left) and LaTiO<sub>3</sub> (right). Dark lines:  $t_{2g}$  bands from the Wannier orbitals on top of the original LDA bands.

Here  $t_{mm'}^{i,i'}$  is the LDA hopping integral from orbital  $m$  on site  $i$  to orbital  $m'$  on site  $i'$ . The operator  $c_{im\sigma}^\dagger$  ( $c_{im\sigma}$ ) creates (annihilates) an electron with spin  $\sigma$  in Wannier state  $m$  at site  $i$ , and  $n_{im\sigma} = c_{im\sigma}^\dagger c_{im\sigma}$ . The parameters  $U$  and  $J$  are the direct and exchange screened Coulomb interactions; we use  $U = 5$  eV and  $J = 0.64$  eV, values which were established in previous works [2,3,31]. As a quantum impurity solver we adopt the generalized hybridization-expansion continuous-time quantum Monte Carlo method [32] in the implementation presented in Ref. [8]. In order to describe the orbital-ordering transition we adopt the approach we introduced in Ref. [4] and used with success for several representative  $e_g$  systems [4,6,7,10]. To extend this to the case of the  $t_{2g}^1$  configuration we define the orbital polarization (the order parameter) as  $p(T) = n_1 - (n_2 + n_3)/2$ , where  $n_i$  are the occupations of the natural orbitals, ordered such that  $n_i \geq n_{i+1}$ . In the high-temperature paraorbital phase  $p(T) \sim 0$ , while in the  $T \rightarrow 0$  limit, i.e., well inside the orbitally ordered phase,  $p(T) \rightarrow 1$ . For the experimental structure, we find

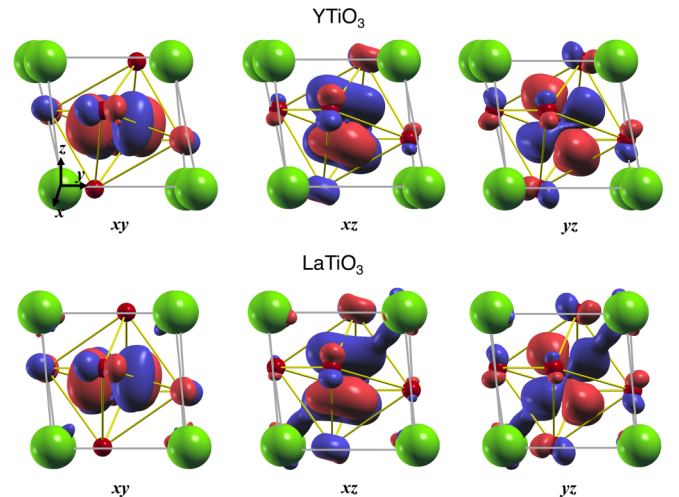


FIG. 3. The  $t_{2g}$ -like Wannier basis for YTiO<sub>3</sub> (top) and LaTiO<sub>3</sub> (bottom).

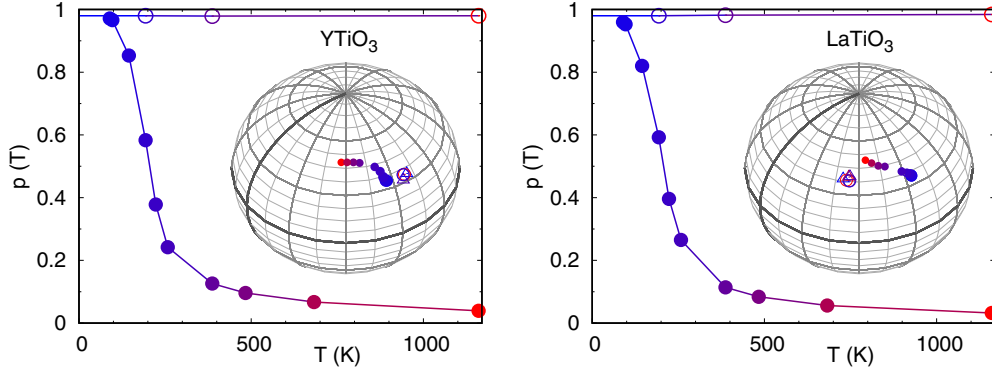


FIG. 4. Superexchange-driven orbital-ordering transition in YTiO<sub>3</sub> (left) and LaTiO<sub>3</sub> (right). The plots show the orbital polarization  $p(T)$  as a function of temperature. Darker symbols correspond to lower temperatures. For each temperature, the most occupied state,  $|\vartheta, \varphi\rangle_1 = \sin \vartheta \cos \varphi |xz\rangle_1 + \cos \vartheta |xy\rangle_1 + \sin \vartheta \sin \varphi |yz\rangle_1$ , is indicated on the sphere in the inset, where the two dark lines correspond to  $\vartheta = 90^\circ$  (equatorial) and  $\varphi = 0^\circ$  (vertical). Open circles: LDA+DMFT results with full crystal-field splitting. Solid circles: results in the zero-crystal-field splitting limit. Triangles: lowest-energy crystal-field orbital from LDA calculations for the experimental structure measured at 2 and 293 K for YTiO<sub>3</sub> (crystal structures from Refs. [11,33]) and 8, 293, and 747 K for LaTiO<sub>3</sub> (crystal structures from Refs. [11,22]).

that the orbital polarization is close to its maximum value already at temperatures as high as 1000 K and changes little with temperature. In the orbitally ordered phase we identify the most occupied natural orbital at site Ti<sub>1</sub> as the state  $|\vartheta, \varphi\rangle = |\vartheta, \varphi\rangle_1 = \sin \vartheta \cos \varphi |xz\rangle_1 + \cos \vartheta |xy\rangle_1 + \sin \vartheta \sin \varphi |yz\rangle_1$ . The corresponding occupied orbitals at sites 2, 3, and 4 can be obtained using point-group symmetries:  $|\vartheta, \varphi\rangle_2 = |\vartheta, 90^\circ - \varphi\rangle_1$ , while  $|\vartheta, \varphi\rangle_3 = |-\vartheta, \varphi\rangle_1$  and  $|\vartheta, \varphi\rangle_4 = |-\vartheta, 90^\circ - \varphi\rangle_1$ . The conclusions so far are in line with established LDA+DMFT results for these materials [2,3].

In order to extract the transition temperature  $T_{\text{KK}}$  for the transition due to only superexchange, we calculate  $p(T)$  for idealized structures. These are obtained by progressively decreasing the effects of the distortions on the on-site energies. We already showed in the past [4,6–8,10] that this approach reliably determines the upper bound for the critical temperature  $T_{\text{KK}}$ , the temperature which determines the onset of the superexchange-driven orbital-ordering transition. The results are discussed in the next section.

### III. RESULTS

The main results obtained via LDA+DMFT calculations are shown in Figs. 4 and 5. Let us start with Fig. 4. Here we display the order parameter  $p(T)$  and, on the sphere, the angles  $\vartheta, \varphi$  identifying the most occupied natural orbital  $|\vartheta, \varphi\rangle$ . These quantities are plotted as a function of temperature for both YTiO<sub>3</sub> and LaTiO<sub>3</sub>. Figure 4 shows that in the presence of crystal-field splitting (open circles) orbital ordering  $p(T) \sim 1$  persists until very high temperatures. This means that, if the structure does not change, no order-to-disorder transition occurs until basically the melting temperature. Also, for both systems the most occupied natural orbital  $|\vartheta, \varphi\rangle$  is essentially temperature independent. This can be seen from the positions of the open symbols on the spheres in Fig. 4. Furthermore,  $|\vartheta, \varphi\rangle$  is close to the corresponding lowest-energy crystal-field state  $|\vartheta_{\text{CF}}, \varphi_{\text{CF}}\rangle$ , shown in the top panels of Fig. 5. The different orbital orderings obtained in the two systems are in good agreement with experiments [34] and can

explain also the fact that LaTiO<sub>3</sub>, at low temperatures, orders antiferromagnetically, while YTiO<sub>3</sub> orders ferromagnetically [3,8]. So far, the conclusions are similar to those for  $e_g$  materials [4,6–8]. In order to quantify the strength of the superexchange interaction, however, we have to analyze the results obtained in the limit of zero crystal-field splitting (solid circles). Figure 4 shows that the superexchange transition occurs at  $T_{\text{KK}} \sim 300$  K. This is a remarkably large value given that the titanates are  $t_{2g}$  systems, comparable [4] to the one for the  $e_g$  system KCuF<sub>3</sub>, although still about half the value of the more covalent system LaMnO<sub>3</sub> [6–8]. There is another important result emphasized in Fig. 4. For YTiO<sub>3</sub>, well below the transition temperature  $T_{\text{KK}}$ , the most occupied natural orbital  $|\vartheta_{\text{KK}}, \varphi_{\text{KK}}\rangle$  is identified by the angles  $\vartheta_{\text{KK}} \sim 60^\circ$  and

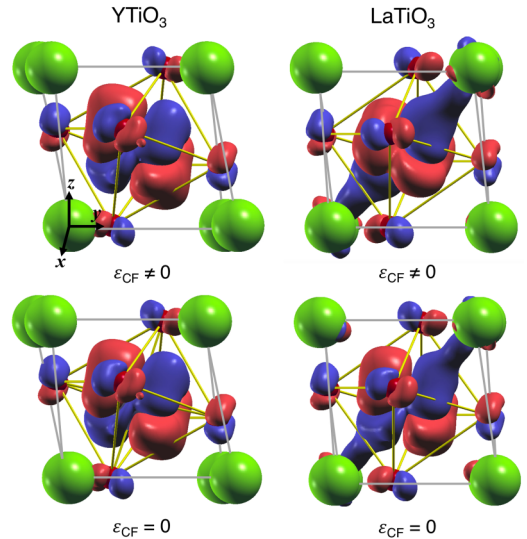


FIG. 5. Top: Lowest-energy crystal-field orbital at site Ti<sub>1</sub>,  $|\vartheta_{\text{CF}}, \varphi_{\text{CF}}\rangle$ . It is very close to the most occupied natural orbital in the presence of the full static crystal-field splitting  $\epsilon_{\text{CF}}$ . Bottom: Most occupied natural orbital  $|\vartheta_{\text{KK}}, \varphi_{\text{KK}}\rangle$  for idealized structure with no static crystal-field splitting in the  $T \rightarrow 0$  limit. Left: YTiO<sub>3</sub>. Right: LaTiO<sub>3</sub>.

$\varphi_{\text{KK}} \sim 90^\circ$ . We therefore obtain  $|\vartheta_{\text{KK}}, \varphi_{\text{KK}}\rangle \sim |\vartheta_{\text{CF}}, \varphi_{\text{CF}}\rangle$ ; this can be seen by comparing the orbitals shown in the top and bottom left panels of Fig. 5. For LaTiO<sub>3</sub> the situation is quite different; the natural orbital  $|\vartheta_{\text{KK}}, \varphi_{\text{KK}}\rangle$  is close to the one we find for YTiO<sub>3</sub>, although with a slightly larger  $\varphi_{\text{KK}} \sim 100^\circ$ . It, however, differs sizably from  $|\vartheta_{\text{CF}}, \varphi_{\text{CF}}\rangle$ , with  $\varphi_{\text{CF}} \sim 50^\circ$ . This can be seen by comparing the orbitals shown in the top and bottom right panels of Fig. 5 or solid and open symbols on the sphere in the right panel of Fig. 4. The state  $|\vartheta_{\text{KK}}, \varphi_{\text{KK}}\rangle$  also differs from predictions based on superexchange models for the idealized cubic perovskite structure [25,27,35–37]. As we will show later, for the ideal cubic structure, the favored orbital in the paramagnetic phase is approximately either  $\frac{1}{\sqrt{3}}|-xz+xy+yz\rangle \sim |55^\circ, 135^\circ\rangle$  or one of the states obtained using the (cubic) symmetry transformations:  $(\vartheta, \varphi) \rightarrow (180^\circ - \vartheta, \varphi)$ ,  $(\vartheta, \varphi - 180^\circ)$ , and  $(180^\circ - \vartheta, \varphi - 180^\circ)$ .

In order to better understand these results, we derive the most general superexchange Hamiltonian for the  $t_{2g}^1$  configuration (paramagnetic phase) and extract its parameters from our LDA+DMFT calculations. To this end, it is convenient to split the superexchange interaction into its irreducible cubic tensor components,

$$\hat{H}_{\text{SE}} = \frac{1}{2} \sum_{ij} \hat{H}_{\text{SE}}^{ij} = \frac{1}{2} \sum_{ij} \sum_{\mu\mu'} \sum_{r,r'} \hat{t}_i^{r,\mu} D_{r\mu,r'\mu'}^{ij} \hat{t}_j^{r',\mu'}. \quad (2)$$

The operator  $\hat{t}_i^{r,\mu}$  is the component  $\mu$  of the tensor operator with rank  $r$  (in this specific case,  $r = 0, 1, 2$ ); for convenience we normalize them such that  $\text{Tr}(\hat{t}_i^{r,\mu})^2 = 1$ . The general analytic expression of the Hamiltonian and the superexchange tensor  $\hat{D}^{ij}$  is given in the Appendix.

In the ideal cubic perovskite case, if one exclusively takes into account the two dominant  $\pi$  bonds, only two orbitals are active in each direction; we define  $t$  as the associated hopping integral, identical for all bonds. In this approximation, for two neighboring sites along  $\hat{z}$ , labeled with  $i$  and  $j = i \pm \hat{z}$ , the superexchange Hamiltonian takes the simple form

$$\begin{aligned} \frac{\hat{H}_{\text{SE}}^{i,j=i\pm\hat{z}}}{2\Gamma_{\text{SE}}} = & -\frac{w_1 + 4w_2}{3} \hat{t}_i^{0,s} \hat{t}_j^{0,s} \\ & + \frac{2w_2 - w_1}{2} \left( \hat{t}_i^{1,z} \hat{t}_j^{1,z} + \frac{1}{3} \hat{t}_i^{2,z^2} \hat{t}_j^{2,z^2} \right) \\ & - \frac{w_1 + w_2}{3\sqrt{2}} (\hat{t}_i^{0,s} \hat{t}_j^{2,z^2} + \tau_i^{2,z^2} \hat{t}_j^{0,s}) \\ & + \frac{w_3 - w_0}{2} \hat{t}_i^{2,x^2-y^2} \hat{t}_j^{2,x^2-y^2} \\ & + \frac{w_3 + w_0}{2} \hat{t}_i^{2,xy} \hat{t}_j^{2,xy}, \end{aligned} \quad (3)$$

where  $\Gamma_{\text{SE}} = 4t^2/U$  is the energy scale. The parameters  $w_i$ , with  $i = 0, \dots, 3$ , can be expressed in terms of the function

$$w(c_1, c_2, c_3) = \frac{c_1}{(1 + 2J/U)} + \frac{c_2}{(1 - J/U)} + \frac{c_3}{(1 - 3J/U)}. \quad (4)$$

More specifically,  $w_0 = w(\frac{1}{3}, -\frac{1}{3}, 0)$ ,  $w_1 = w(\frac{1}{3}, \frac{2}{3}, 0)$ ,  $w_2 = w(0, \frac{1}{4}, \frac{3}{4})$ , and  $w_3 = w(0, 0, 1)$ . The corresponding

Hamiltonian for neighbors along the  $\hat{x}$  direction is

$$\begin{aligned} \frac{\hat{H}_{\text{SE}}^{i,j=i\pm\hat{x}}}{2\Gamma_{\text{SE}}} = & -\frac{w_1 + 4w_2}{3} \hat{t}_i^{0,s} \hat{t}_j^{0,s} \\ & + \frac{2w_2 - w_1}{4} \left( \hat{t}_i^{1,z} \hat{t}_j^{1,z} + \frac{5}{3} \hat{t}_i^{2,z^2} \hat{t}_j^{2,z^2} \right) \\ & + \frac{w_1 + w_2}{6\sqrt{2}} (\hat{t}_i^{0,s} \hat{t}_j^{2,z^2} + \tau_i^{2,z^2} \hat{t}_j^{0,s}) \\ & + s \frac{2w_2 - w_1}{4\sqrt{3}} (\hat{t}_i^{1,z} \hat{t}_j^{2,z^2} + \tau_i^{2,z^2} \hat{t}_j^{1,z}) \\ & - s \frac{w_1 + w_2}{2\sqrt{6}} (\hat{t}_i^{0,s} \hat{t}_j^{1,z} + \tau_i^{1,z} \hat{t}_j^{0,s}) \\ & + \frac{w_3 - w_0}{4} (\hat{t}_i^{1,x} \hat{t}_j^{1,x} + \hat{t}_i^{2,xz} \hat{t}_j^{2,xz}) \\ & + s \frac{w_3 - w_0}{4} (\hat{t}_i^{2,xz} \hat{t}_j^{1,x} + \hat{t}_i^{1,x} \hat{t}_j^{2,xz}) \\ & + \frac{w_3 + w_0}{4} (\hat{t}_i^{1,y} \hat{t}_j^{1,y} + \hat{t}_i^{2,yz} \hat{t}_j^{2,yz}) \\ & + s \frac{w_3 + w_0}{4} (\hat{t}_i^{1,y} \hat{t}_j^{2,yz} + \hat{t}_i^{2,yz} \hat{t}_j^{1,y}), \end{aligned} \quad (5)$$

where  $s = 1$ . The superexchange Hamiltonian in the  $\hat{y}$  direction  $\hat{H}_{\text{SE}}^{i,j=i\pm\hat{y}}$  can be obtained from the expression for  $\hat{H}_{\text{SE}}^{i,j=i\pm\hat{x}}$  by setting  $s = -1$ . In this idealized case, under the local constraint  $n_{xy} + n_{xz} + n_{yz} = 1$ , the superexchange Hamiltonian given above can be recast into a simpler form in terms of spin-1/2 pseudospin operators [21,36,37]. For a supercell compatible with the GdFeO<sub>3</sub>-type distortion the associated classical orbitally ordered ground state is associated with a  $D_{3d}$  octahedral distortion [25], i.e., approximately the  $\frac{1}{\sqrt{3}}|-xz+xy+yz\rangle$  state. In the formalism just introduced, this type of ordering arises from the terms  $\hat{t}_i^{2,xz} \hat{t}_j^{2,xz}$  in  $\hat{H}_{\text{SE}}^{i,j=i\pm\hat{x}}$  and  $\hat{H}_{\text{SE}}^{i,j=i\pm\hat{y}}$ .

The general form of the interaction given in Eq. (2) allows us to go from simple models to realistic superexchange Hamiltonians with general hopping integrals. The full expression for the coupling constants in Eq. (2) can be found in the Appendix.

In Fig. 6 we show  $\Delta E(\vartheta, \varphi)$ , the classical superexchange energy gain per cell for orbital ordering compatible with the space group of the titanates. It is defined as

$$\Delta E(\vartheta, \varphi) = \frac{1}{N} \sum_{j>i} (\langle \Psi_{ij}^{OO} | \hat{H}_{\text{SE}}^{ij} | \Psi_{ij}^{OO} \rangle - E_0^{ij}), \quad (6)$$

where  $|\Psi_{ij}^{OO}\rangle = |\vartheta, \varphi\rangle_i |\vartheta, \varphi\rangle_j$  and the energy zero  $E_0^{ij}$  is the superexchange energy for the paraorbital state. The terms of Hamiltonian (2) which can give rise to an orbital-ordering transition are those which are quadratic in the operators with rank  $r > 0$ . The linear terms instead yield an orbital Zeeman effect [10], and their contributions cancel out in the ideal cubic limit; this can be seen by comparing the top and bottom right panels of Fig. 6. Figure 6 also shows that in the cubic perovskite limit the superexchange energy gain for a classical orbitally ordered state  $\Delta E(\vartheta, \varphi)$  is, as expected, very small even for the optimal angles. This is because all superexchange terms except the one arising from  $\hat{t}_i^{2,xz} \hat{t}_j^{2,xz}$  are either frustrated or cancel out (see the Appendix for details),

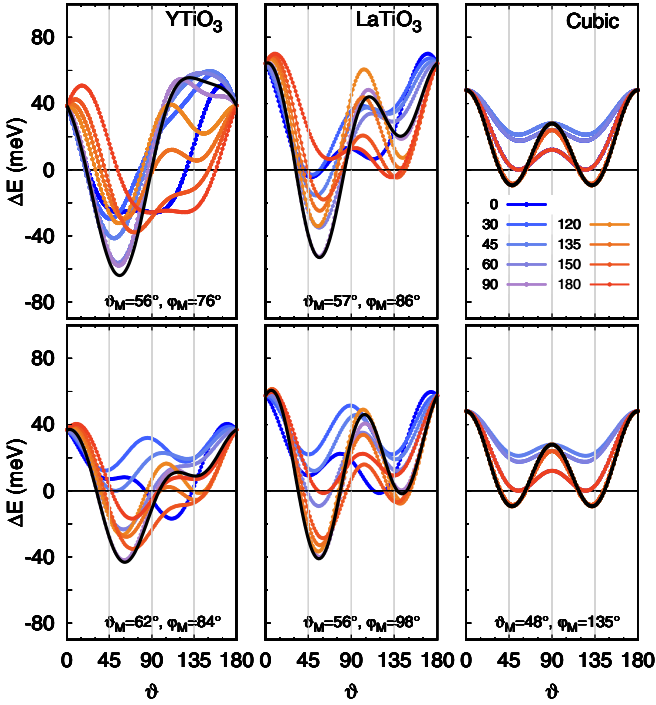


FIG. 6. Superexchange total energy gain  $\Delta E(\vartheta, \varphi)$  for a classical orbitally ordered ground state compatible with the GdFeO<sub>3</sub>-type distortion. The energy zero is the energy of the paraorbital state. In each panel, the different lines correspond to the values of  $\varphi$  specified in the top right panel. Top: all superexchange terms. Bottom: only quadratic terms. Left: YTiO<sub>3</sub>. Middle: LaTiO<sub>3</sub>. Right: For comparison, we show the result for the cubic case. We chose  $t \sim 150$  meV, which is a value representative for LaTiO<sub>3</sub> and YTiO<sub>3</sub>, see Table I. Black lines:  $\varphi$  values that yield the energy minimum, indicated in each case. The results are invariant under the transformation  $(\vartheta, \varphi) \rightarrow (180^\circ - \vartheta, \varphi - 180^\circ)$ ; hence, we show only results for  $\vartheta$  and  $\varphi$  between  $0^\circ$  and  $180^\circ$ . In the cubic limit an additional symmetry is present,  $(\vartheta, \varphi) \rightarrow (180^\circ - \vartheta, \varphi)$ .

so that

$$\frac{\Delta E(\vartheta, \varphi)}{2\Gamma_{SE}} = \frac{2w_2 - w_1}{24} (1 + 3 \cos 2\vartheta)^2 + \frac{w_3 - w_0}{4} \times \left[ \sin^2 2\vartheta \sin 2\varphi + \frac{1}{4} (1 - \cos 2\vartheta)^2 \sin^2 2\varphi \right]. \quad (7)$$

Furthermore, it has been pointed out that in such a limit quantum fluctuations might even completely prevent ordering at finite temperature [38]. These considerations are completely in line with known results for the pseudospin-1/2 model [21,22,25,35–37].

In the presence of the GdFeO<sub>3</sub>-type distortion, however, the hopping integrals couple different orbitals, and the simple pseudospin-1/2 picture no longer applies in general. Earlier modelizations for the magnetic phase [27,28,35,39] already showed that the GdFeO<sub>3</sub>-type distortion can introduce new superexchange paths, e.g., in a simple tight-binding description, via the coupling of atomic  $e_g$  and  $t_{2g}$  states, thus influencing spin-orbital ordering phenomena. Thanks to the general superexchange Hamiltonian, Eq. (2), and the realistic estimates of the superexchange parameters obtained in this work via the

TABLE I. Hopping integrals  $-t_{m,m'}^{i,i'}/\text{meV}$  from site  $i$  of type Ti<sub>1</sub> to site  $i' = i + lx + my + nz$  of type Ti<sub>2</sub> or Ti<sub>3</sub>. YTiO<sub>3</sub>, LaTiO<sub>3</sub>, and the ideal cubic limit are given from left to right. In the notation adopted, the  $(xz, yz, xy)$  Wannier basis changes from site to site due to symmetries. Point symmetry transformations with respect to site Ti<sub>1</sub> are  $(\hat{x} \leftrightarrow \hat{y})$  for Ti<sub>2</sub> and  $(\hat{z} \leftrightarrow -\hat{z})$  for Ti<sub>3</sub>.

		YTiO <sub>3</sub>			LaTiO <sub>3</sub>			Cubic		
		$lmn$			$lmn$			$lmn$		
$m_1$	$m'_1$	001	010	100	001	010	100	001	010	100
$xy_1$	$xy'_1$	-5	-151	-151	-16	-174	-174	0	-t	-t
$xz_1$	$xz'_1$	162	-43	-43	198	-39	-39	-t	0	0
$yz_1$	$yz'_1$	46	63	63	180	77	77	-t	0	0
$xy_1$	$xz'_1$	82	-64	70	51	-60	73	0	0	0
$xz_1$	$xy'_1$	82	70	-64	51	73	-60	0	0	0
$xy_1$	$yz'_1$	-66	-18	-50	-61	-29	-39	0	0	0
$yz_1$	$xy'_1$	-66	-50	-18	-61	-39	-29	0	0	0
$xz_1$	$yz'_1$	73	30	-182	52	12	-176	0	0	-t
$yz_1$	$xz'_1$	73	-182	30	52	-176	12	0	-t	0

expressions given in the Appendix, we can now quantify this effect and specify its nature. Furthermore, this can be done specifically for the paramagnetic phase, the one relevant for unraveling the role of the superexchange interaction in the genesis of orbital ordering at the temperatures where it sets in.

In the left and middle panels of Fig. 6 we show  $\Delta E(\vartheta, \varphi)$  for realistic hopping integrals; the values of the latter can be found in Table I. The top panels show the total energy gain, and the bottom panels show the contribution of only the quadratic terms, those that can give rise to a phase transition. The angles  $\vartheta_M, \varphi_M$  that maximize the energy gain, yielding  $\Delta E(\vartheta_M, \varphi_M) = \Delta E_M$ , are basically the same with and without linear terms. Furthermore,  $\vartheta_M$  and  $\varphi_M$  are in accord with  $\vartheta_{KK}$  and  $\varphi_{KK}$  obtained in LDA+DMFT calculations. The energy gain at the optimal angles is  $\Delta E_M \sim 40$  meV, also in line with the critical temperature of about 300 K obtained in LDA+DMFT calculations, taking into account that  $\Delta E_M$  is overestimated due to the neglected dynamical quantum effects. This energy gain is about 5 times larger than the corresponding result in the cubic limit (right panels). By analyzing these results we find that it is the off-diagonal hopping integrals that enhance the superexchange energy gain, favoring a Jahn-Teller-like natural orbital with  $\varphi_{KK} \sim 90^\circ$  over the  $\frac{1}{\sqrt{3}}|-xz + xy + yz\rangle$  natural orbital with  $\varphi_{KK} = 135^\circ$ . The superexchange terms that turn out to contribute most, in addition to  $\hat{t}_i^{2,xz}\hat{t}_j^{2,xz}$ , are  $\hat{t}_j^{1,z}\hat{t}_i^{2,xz}$  and  $\hat{t}_j^{1,z}\hat{t}_j^{1,x}$ , as well as  $\hat{t}_i^{2,xz}\hat{t}_j^{1,x}$ . This can be understood from Table I, which shows the changes in hopping integrals with respect to the cubic limit, and Tables II and III, which show the superexchange tensor elements as a function of the hopping integrals. This conclusion applies to both LaTiO<sub>3</sub> and YTiO<sub>3</sub>, with the angle  $\varphi_{KK}$  being slightly smaller than  $90^\circ$  in the case of YTiO<sub>3</sub> and slightly larger for LaTiO<sub>3</sub>. Figures 5 and 6, however, also emphasize the main difference between YTiO<sub>3</sub> and LaTiO<sub>3</sub>: while superexchange effects are rather similar in the two systems, in YTiO<sub>3</sub> they reinforce the effect of the static crystal-field splitting. Instead, in LaTiO<sub>3</sub>, which has a smaller GdFeO<sub>3</sub>-type distortion, they partially compete with it.

TABLE II. Tensor elements different from zero in the case in which the hopping integrals are only diagonal.

$r \mu$	$r' \mu'$	$D_{r\mu, r'\mu'}^{ij}$	$r \mu$	$r' \mu'$	$D_{r\mu, r'\mu'}^{ij}$
0 $s$	0 $s$	$-\frac{4}{U} \frac{w_1+4w_2}{3} (t_{xz,xz}^2 + t_{yz,yz}^2 + t_{xy,xy}^2)$	1 $z$	1 $z$	$+\frac{4}{U} \frac{2w_2-w_1}{2} (t_{xz,xz}^2 + t_{yz,yz}^2)$
2 $z^2$	2 $z^2$	$+\frac{4}{U} \frac{2w_2-w_1}{6} (t_{xz,xz}^2 + t_{yz,yz}^2 + 4t_{xy,xy}^2)$	0 $s$	1 $z$	$-\frac{4}{U} \frac{w_1+w_2}{\sqrt{6}} (t_{xz,xz}^2 - t_{yz,yz}^2)$
0 $s$	2 $z^2$	$-\frac{4}{U} \frac{w_1+w_2}{3\sqrt{2}} (t_{xz,xz}^2 + t_{yz,yz}^2 - 2t_{xy,xy}^2)$	1 $z$	2 $z^2$	$+\frac{4}{U} \frac{2w_2-w_1}{2\sqrt{3}} (t_{xz,xz}^2 - t_{yz,yz}^2)$
1 $x$	1 $x$	$+\frac{4}{U} \frac{w_3-w_0}{2} (t_{xz,xz} + t_{yz,yz})t_{xy,xy}$	1 $y$	1 $y$	$+\frac{4}{U} \frac{w_0+w_3}{2} (t_{xz,xz} + t_{yz,yz})t_{xy,xy}$
2 $xz$	2 $xz$	$+\frac{4}{U} \frac{w_3-w_0}{2} (t_{xz,xz} + t_{yz,yz})t_{xy,xy}$	2 $yz$	2 $yz$	$+\frac{4}{U} \frac{w_0+w_3}{2} (t_{xz,xz} + t_{yz,yz})t_{xy,xy}$
2 $x^2-y^2$	2 $x^2-y^2$	$+\frac{8}{U} \frac{w_3-w_0}{2} t_{xz,xz}t_{yz,yz}$	2 $xy$	2 $xy$	$+\frac{8}{U} \frac{w_0+w_3}{2} t_{xz,xz}t_{yz,yz}$
1 $x$	2 $xz$	$+\frac{4}{U} \frac{w_3-w_0}{2} (t_{xz,xz} - t_{yz,yz})t_{xy,xy}$	1 $y$	2 $xz$	$+\frac{4}{U} \frac{w_0+w_3}{2} (t_{xz,xz} - t_{yz,yz})t_{xy,xy}$

Summarizing, in both LaTiO<sub>3</sub> and YTiO<sub>3</sub>, our results show that pure superexchange effects leading to orbital ordering are much larger than expected from idealized cubic perovskite models. Still, the upper limit for the superexchange critical temperature, although large, is, at most,  $T_{KK} \sim 300$  K. Orbital order at higher temperature can thus be ascribed only to the presence of a static crystal-field splitting. In this respect, a systematic experimental study of the evolution of distortions with increasing temperature well above 300 K would be essential to finally settle the question of the role of superexchange in the genesis of orbital ordering. Some high-temperature data are available for LaTiO<sub>3</sub>. They indicate that all distortions (Jahn-Teller, tilting and rotation angles, and the  $D_{3d}$  distortions) either remain unchanged or slightly decrease with increasing temperature. The available structural data have been obtained with different techniques [11,22,33], and their accuracy might

not be directly comparable; nevertheless, based on them, we find that the lowest-energy LDA crystal-field orbital does not change much with increasing temperature. The corresponding LDA+DMFT results are shown in Fig. 4. This indicates that orbital ordering stays almost unchanged well above 300 K. If this is experimentally confirmed in both materials, it would show that the superexchange interaction, although unexpectedly strong, cannot drive orbital-order alone in the titanates. This conclusion would then be close to the one we previously obtained for LaMnO<sub>3</sub> and KCuF<sub>3</sub> and other representative  $e_g$  cases [4,6–10]. It is reinforced by the fact that, while the superexchange interaction appears to cooperate with crystal-field effects in YTiO<sub>3</sub>, in LaTiO<sub>3</sub> it partially competes with them, with both being orbitally ordered. Finally, the fact that the classical superexchange energy gain for static orbital ordering is enhanced by about a factor of 5 in the presence

TABLE III. Additional quadratic ( $r \neq 0, r' \neq 0$ ) and linear terms ( $r = 0, r' \neq 0$ ) present if the off-diagonal hopping integrals are nonzero. Only relevant contributions are listed; here we assume for simplicity that the hopping integrals are real, as in the case considered in this paper.

$r \mu$	$r' \mu'$	$D_{r\mu, r'\mu'}^{ij}$
1 $z$	1 $z$	$-\frac{4}{U} \frac{2w_2-w_1}{2} (t_{xz,yz}^2 + t_{yz,xz}^2)$
1 $z$	2 $z^2$	$+\frac{4}{U} \frac{2w_2-w_1}{2\sqrt{3}} [t_{xz,yz}^2 - t_{yz,xz}^2 - 2(t_{xz,xy}^2 - t_{yz,xy}^2)]$
2 $z^2$	2 $z^2$	$+\frac{4}{U} \frac{2w_2-w_1}{6} [t_{xz,yz}^2 + t_{yz,xz}^2 - 2(t_{xz,xy}^2 + t_{xy,xz}^2 + t_{yz,xy}^2 + t_{xy,yz}^2) + 4t_{xy,xy}^2]$
1 $z$	1 $x$	$+\frac{4}{U} \frac{2w_2+w_3-w_1-w_0}{2\sqrt{2}} [(t_{xz,xz} + t_{xz,yz})t_{xz,xy} - (t_{yz,xz} + t_{yz,yz})t_{yz,xy}]$
1 $z$	2 $xz$	$+\frac{4}{U} \frac{2w_2+w_3-w_1-w_0}{2\sqrt{2}} [(t_{xz,xz} - t_{xz,yz})t_{xz,xy} - (t_{yz,xz} - t_{yz,yz})t_{yz,xy}]$
1 $z$	2 $x^2-y^2$	$+\frac{4}{U} \frac{2w_2+w_3-w_1-w_0}{2} (t_{xz,xz}t_{xz,yz} - t_{yz,xz}t_{yz,yz})$
2 $z^2$	1 $x$	$+\frac{4}{U} \frac{2w_2+w_3-w_1-w_0}{2\sqrt{6}} [(t_{xz,xz} + t_{xz,yz})t_{xz,xy} + (t_{yz,xz} + t_{yz,yz})t_{yz,xy} - 2(t_{xy,xz} + t_{xy,yz})t_{xy,xy}]$
2 $z,^2$	2 $xz$	$+\frac{4}{U} \frac{2w_2+w_3-w_1-w_0}{2\sqrt{6}} [(t_{xz,xz} - t_{xz,yz})t_{xz,xy} + (t_{yz,xz} - t_{yz,yz})t_{yz,xy} - 2(t_{xy,xz} - t_{xy,yz})t_{xy,xy}]$
2 $z^2$	2 $x^2-y^2$	$+\frac{4}{U} \frac{2w_2+w_3-w_1-w_0}{2\sqrt{3}} (t_{xz,xz}t_{xz,yz} + t_{yz,xz}t_{yz,yz} - 2t_{xy,xz}t_{xy,yz})$
1 $x$	1 $x$	$+\frac{4}{U} \frac{w_3-w_0}{2} [(t_{xz,yz} + t_{yz,xz})t_{xy,xy} + (t_{xz,xy} + t_{yz,xy})(t_{xy,xz} + t_{xy,yz})]$
1 $x$	2 $xz$	$+\frac{4}{U} \frac{w_3-w_0}{2} [(-t_{xz,yz} + t_{yz,xz})t_{xy,xy} + (t_{xz,xy} + t_{yz,xy})(t_{xy,xz} - t_{xy,yz})]$
2 $xz$	2 $xz$	$-\frac{4}{U} \frac{w_3-w_0}{2} [(t_{xz,yz} + t_{yz,xz})t_{xy,xy} - (t_{xz,xy} - t_{yz,xy})(t_{xy,xz} - t_{xy,yz})]$
2 $x^2-y^2$	2 $x^2-y^2$	$+\frac{8}{U} \frac{w_3-w_0}{2} t_{xz,yz}t_{yz,xz}$
1 $x$	2 $x^2-y^2$	$+\frac{8}{U} \frac{w_3-w_0}{2\sqrt{2}} [(t_{xz,xz} + t_{yz,xz})t_{xy,yz} + (t_{xz,yz} + t_{yz,yz})t_{xy,xz}]$
2 $xz$	2 $x^2-y^2$	$+\frac{8}{U} \frac{w_3-w_0}{2\sqrt{2}} [(t_{xz,xz} - t_{yz,xz})t_{xy,yz} + (t_{xz,yz} - t_{yz,yz})t_{xy,xz}]$
0 $s$	1 $x$	$-\frac{4}{U} \frac{4w_2-w_3+w_1+w_0}{2\sqrt{3}} [(t_{xz,xz} + t_{xz,yz})t_{xz,xy} + (t_{yz,xz} + t_{yz,yz})t_{yz,xy} + (t_{xy,xz} + t_{xy,yz})t_{xy,xy}]$
0 $s$	1 $z$	$-\frac{4}{U} \frac{w_1+w_2}{\sqrt{6}} (t_{yz,xz}^2 + t_{xz,xz}^2 - t_{xz,yz}^2 - t_{xy,yz}^2)$
0 $s$	2 $xz$	$-\frac{4}{U} \frac{4w_2-w_3+w_1+w_0}{2\sqrt{3}} [(t_{xz,xz} - t_{xz,yz})t_{xz,xy} + (t_{yz,xz} - t_{yz,yz})t_{yz,xy} + (t_{xy,xz} - t_{xy,yz})t_{xy,xy}]$
0 $s$	2 $x^2-y^2$	$-\frac{4}{U} \frac{4w_2-w_3+w_1+w_0}{\sqrt{6}} (t_{xz,xz}t_{xz,yz} + t_{yz,xz}t_{yz,yz} + t_{xy,xz}t_{xy,yz})$
0 $s$	2 $z^2$	$-\frac{4}{U} \frac{w_1+w_2}{3\sqrt{2}} (t_{yz,xz}^2 + t_{xz,xz}^2 + t_{xz,yz}^2 + t_{xy,yz}^2 - 2t_{xz,xy}^2 - 2t_{xy,yz}^2)$

of the GdFeO<sub>3</sub>-type distortion so that  $T_{\text{KK}}$  is, surprisingly, about as large as in KCuF<sub>3</sub> supports the view that processes involving dynamical orbital fluctuations are not likely to play a role in determining the orbital physics of either system.

#### IV. CONCLUSIONS

We have studied the role of superexchange in the origin of orbital ordering in representative  $t_{2g}$  materials, YTiO<sub>3</sub> and LaTiO<sub>3</sub>. We adopted an approach that we previously established and successfully used for  $e_g$  systems [4,6–8]. We find that the superexchange transition temperature is, surprisingly, as large as in the case of KCuF<sub>3</sub>, a paradigmatic  $e_g$  orbitally ordered material. We show it is strongly enhanced by the GdFeO<sub>3</sub>-type distortion. While in the case of YTiO<sub>3</sub> the superexchange most occupied orbital  $|\vartheta_{\text{KK}}, \varphi_{\text{KK}}\rangle$  is similar to the lowest-energy crystal-field state  $|\vartheta_{\text{CF}}, \varphi_{\text{CF}}\rangle$ , in LaTiO<sub>3</sub> they differ substantially. This indicates that in YTiO<sub>3</sub> lattice distortions reinforce superexchange effects, while in the case of LaTiO<sub>3</sub> the two effects compete. High-temperature structural data are, to the best of our knowledge, available for only LaTiO<sub>3</sub> so far. They indicate no substantial change in the occupied orbital up to 700 K, i.e., well above  $T_{\text{KK}}$ . Orbital ordering persisting until that temperature cannot be explained by the superexchange mechanism alone and needs the explicit presence of static crystal-field splitting. This conclusion is reinforced by the fact that in LaTiO<sub>3</sub> the superexchange most occupied natural orbital differs substantially from the experimental one.

#### ACKNOWLEDGEMENT

The authors gratefully acknowledge computational grants on the Jülich supercomputers JUWELS (NIC) and JURECA (JARA).

#### APPENDIX: ORBITAL SUPEREXCHANGE FOR $t_{2g}^1$ SYSTEMS

Here we give the general form of the superexchange interaction, expressed as a function of orbital irreducible cubic tensor operators  $\hat{\tau}_i^{r,\mu}$  of rank  $r = 0, 1, 2$ , with components  $\mu = -r, \dots, r$ ,

$$\hat{H}_{\text{SE}} = \frac{1}{2} \sum_{ij} \sum_{\mu\mu'} \sum_{r,r'} \hat{\tau}_i^{r,\mu} D_{r\mu,r'\mu'}^{ij} \hat{\tau}_j^{r',\mu'}. \quad (\text{A1})$$

We obtain the superexchange Hamiltonian from second-order perturbation theory and project it into its irreducible tensor components. For convenience we chose the normalization of the tensor operators such that  $\text{Tr}(\hat{\tau}_i^{r,\mu})^2 = 1$  and split the expression of the tensor elements appearing in Eq. (A1) in two terms,

$$D_{r\mu,r'\mu'}^{ij} = B_{r\mu,r'\mu'}^{ij} + C_{r\mu,r'\mu'}^{ij}. \quad (\text{A2})$$

The first term is

$$B_{r\mu,r'\mu'}^{ij} = -2 \sum_{abcd} \langle a | \hat{\tau}_i^{r,\mu} | c \rangle \langle b | \hat{\tau}_j^{r',\mu'} | d \rangle \frac{t_{c,d}^{i,j} \overline{t_{a,b}^{i,j}}}{U} \times [w_1(\delta_{\mu',0} + \delta_{\mu,0}) + w_0(2 - \delta_{\mu',0} - \delta_{\mu,0})], \quad (\text{A3})$$

and the second is

$$C_{r\mu,r'\mu'}^{ij} = -4 \sum_{abcd} \langle a | \hat{\tau}_i^{r,\mu} | c \rangle \langle d | \hat{\tau}_j^{r',\mu'} | b \rangle \times \left\{ w_2 \sum_{m_1} \left( \delta_{\mu'r,0s} \frac{t_{c,m_1}^{i,j} \overline{t_{a,m_1}^{i,j}}}{U} + \delta_{\mu r,0s} \frac{t_{m_1,b}^{i,j} \overline{t_{m_1,d}^{i,j}}}{U} \right) - \frac{t_{c,d}^{i,j} \overline{t_{a,b}^{i,j}}}{U} \left[ w_2(\delta_{\mu',0} + \delta_{\mu,0}) + \frac{w_3}{2}(2 - \delta_{\mu,0} - \delta_{\mu',0}) \right] \right\}, \quad (\text{A4})$$

where  $a, b, c, d$  are  $t_{2g}$  states. The parameters  $w_i$ , with  $i = 0, \dots, 3$ , can be expressed as  $w_0 = w(\frac{1}{3}, -\frac{1}{3}, 0)$ ,  $w_1 = w(\frac{1}{3}, \frac{2}{3}, 0)$ ,  $w_2 = w(0, \frac{1}{4}, \frac{3}{4})$ , and  $w_3 = w(0, 0, 1)$ , where

$$w(c_1, c_2, c_3) = \frac{c_1}{1 + 2J/U} + \frac{c_2}{1 - J/U} + \frac{c_3}{1 - 3J/U}. \quad (\text{A5})$$

In the special case of diagonal hopping integrals the only terms which are nonzero are those given in Table II. For bonds in the  $\hat{x}$  direction we thus have, for  $j = i \pm \hat{x}$ ,

$$\begin{aligned} \hat{H}_{\text{SE}}^{i,j} = & -\frac{4(t_{xz,xz}^2 + t_{xy,xy}^2)}{U} \frac{w_1 + 4w_2}{3} \hat{\tau}_i^{0,s} \hat{\tau}_j^{0,s} \\ & + \frac{4t_{xz,xz}^2}{U} \frac{2w_2 - w_1}{2} \hat{\tau}_i^{1,z} \hat{\tau}_j^{1,z} \\ & + \frac{4(t_{xz,xz}^2 + 4t_{xy,xy}^2)}{U} \frac{2w_2 - w_1}{6} \hat{\tau}_i^{2,z^2} \hat{\tau}_j^{2,z^2} \\ & + \frac{4(2t_{xy,xy}^2 - t_{xz,xz}^2)}{U} \frac{w_1 + w_2}{3\sqrt{2}} (\hat{\tau}_i^{0,s} \hat{\tau}_j^{2,z^2} + \tau_i^{2,z^2} \hat{\tau}_j^{0,s}) \\ & + s_x \frac{2t_{xz,xz}^2}{U} \frac{2w_2 - w_1}{\sqrt{3}} (\hat{\tau}_i^{1,z} \hat{\tau}_j^{2,z^2} + \tau_i^{2,z^2} \hat{\tau}_j^{1,z}) \\ & - s_x \frac{4t_{xz,xz}^2}{U} \frac{w_1 + w_2}{\sqrt{6}} (\hat{\tau}_i^{0,s} \hat{\tau}_j^{1,z} + \tau_i^{1,z} \hat{\tau}_j^{0,s}) \\ & + \frac{4t_{xz,xz} t_{xy,xy}}{U} \frac{w_3 - w_0}{2} (\hat{\tau}_i^{1,x} \hat{\tau}_j^{1,x} + \hat{\tau}_i^{2,xz} \hat{\tau}_j^{2,xz}) \\ & + s_x \frac{4t_{xz,xz} t_{xy,xy}}{U} \frac{w_3 - w_0}{2} (\hat{\tau}_i^{2,xz} \hat{\tau}_j^{1,x} + \hat{\tau}_i^{1,x} \hat{\tau}_j^{2,xz}) \\ & + \frac{4t_{xz,xz} t_{xy,xy}}{U} \frac{w_3 + w_0}{2} (\hat{\tau}_i^{1,y} \hat{\tau}_j^{1,y} + \hat{\tau}_i^{2,yz} \hat{\tau}_j^{2,yz}) \\ & + s_x \frac{4t_{xz,xz} t_{xy,xy}}{U} \frac{w_3 + w_0}{2} (\hat{\tau}_i^{1,y} \hat{\tau}_j^{2,yz} + \hat{\tau}_i^{2,yz} \hat{\tau}_j^{1,y}), \quad (\text{A6}) \end{aligned}$$

where  $s_x = 1$ . The superexchange Hamiltonian  $H_{\text{SE}}^{i,j=i\pm\hat{y}}$  can be obtained using symmetries, i.e., by exchanging in the prefactors  $x \leftrightarrow y$  and setting  $s_y = -s_x$ . Next, we define  $p_{r,\mu} = \langle i | \vartheta, \varphi | \hat{\tau}_i^{r,\mu} | \vartheta, \varphi \rangle_i$ . The relevant nonzero terms are, for  $i$  corresponding to site Ti<sub>1</sub> (see Fig. 1),

$$p_{1,z} = (1 - \cos 2\vartheta) \cos 2\phi / 2\sqrt{2}, \quad (\text{A7})$$

$$p_{1,x} = \sin 2\vartheta (\cos \varphi + \sin \varphi) / 2, \quad (\text{A8})$$

$$p_{2,z^2} = -(1 + 3 \cos 2\vartheta) / 2\sqrt{6}, \quad (\text{A9})$$

$$p_{2,xz} = \sin 2\vartheta (\cos \varphi - \sin \varphi)/2, \quad (\text{A10})$$

$$p_{2,x^2-y^2} = (1 - \cos 2\vartheta) \sin 2\varphi / 2\sqrt{2}. \quad (\text{A11})$$

If only diagonal hopping integrals are present, the classical energy associated with orbital order compatible with the space group of the titanates is thus  $\Delta E(\vartheta, \varphi) = \Delta E_Q(\vartheta, \varphi) + \Delta E_L(\vartheta, \varphi)$ , where the quadratic term is

$$\begin{aligned} \Delta E_Q(\vartheta, \varphi) = & \frac{4(t_{xz,xz}^2 + t_{yz,yz}^2 + 4t_{xy,xy}^2)}{U} \frac{2w_2 - w_1}{3} p_{2,z^2}^2 \\ & + \frac{4(t_{xz,xz} + t_{yz,yz})t_{xy,xy}}{U} \frac{w_3 - w_0}{2} (p_{1,x}^2 - p_{2,xz}^2) \\ & + \frac{8t_{xz,xz}t_{yz,yz}}{U} \frac{w_3 - w_0}{2} p_{2,x^2-y^2}^2 \\ & - \frac{4(t_{xz,xz}^2 - t_{yz,yz}^2)}{U} \frac{2w_2 - w_1}{\sqrt{3}} p_{1,z}p_{2,z^2} \\ & + \frac{8(t_{xz,xz} - t_{yz,yz})t_{xy,xy}}{U} \frac{w_3 + w_0}{2} p_{1,x}p_{2,xz}, \end{aligned} \quad (\text{A12})$$

and the linear term is

$$\begin{aligned} \Delta E_L(\vartheta, \varphi) = & - \frac{16(t_{xz,xz}^2 + t_{yz,yz}^2 - 2t_{xy,xy}^2)}{U} \frac{w_1 + w_2}{3\sqrt{6}} p_{2,z^2} \\ & + \frac{8(t_{xz,xz}^2 - t_{yz,yz}^2)}{U} \frac{w_1 + w_2}{\sqrt{18}} p_{1,z}. \end{aligned} \quad (\text{A13})$$

In the cubic limit, in which all nonzero hopping integrals are identical, all linear and some of the quadratic terms cancel, and this further simplifies to

$$\begin{aligned} \frac{\Delta E(\vartheta, \varphi)}{2\Gamma_{SE}} = & (2w_2 - w_1)p_{2,z^2}^2 \\ & + \frac{w_3 - w_0}{2} (p_{1,x}^2 - p_{2,xz}^2 + p_{2,x^2-y^2}^2), \end{aligned} \quad (\text{A14})$$

where  $\Gamma_{SE} = \frac{4t^2}{U}$ . Hence, in this case, only the  $\hat{t}_{2xz}^i \hat{t}_{2xz}^j$  term yields an actual energy gain.

- 
- [1] J. Kanamori, *J. Appl. Phys.* **31**, S14 (1960).  
[2] E. Pavarini, S. Biermann, A. Poteryaev, A. I. Lichtenstein, A. Georges, and O. K. Andersen, *Phys. Rev. Lett.* **92**, 176403 (2004).  
[3] E. Pavarini, A. Yamasaki, J. Nuss, and O. K. Andersen, *New J. Phys.* **7**, 188 (2005).  
[4] E. Pavarini, E. Koch, and A. I. Lichtenstein, *Phys. Rev. Lett.* **101**, 266405 (2008).  
[5] K. I. Kugel' and D. I. Khomskii, *Zh. Eksp. Teor. Fiz.* **64**, 1429 (1973) [*Sov. Phys. JETP* **37**, 725 (1973)].  
[6] E. Pavarini and E. Koch, *Phys. Rev. Lett.* **104**, 086402 (2010).  
[7] A. Flesch, G. Zhang, E. Koch, and E. Pavarini, *Phys. Rev. B* **85**, 035124 (2012).  
[8] A. Flesch, E. Gorelov, E. Koch, and E. Pavarini, *Phys. Rev. B* **87**, 195141 (2013).  
[9] H. Sims, E. Pavarini, and E. Koch, *Phys. Rev. B* **96**, 054107 (2017).  
[10] J. Musshoff, G. Zhang, E. Koch, and E. Pavarini, *Phys. Rev. B* **100**, 045116 (2019).  
[11] A. C. Komarek, H. Roth, M. Cwik, W.-D. Stein, J. Baier, M. Kriener, F. Bouree, T. Lorenz, and M. Braden, *Phys. Rev. B* **75**, 224402 (2007).  
[12] M. Imada, A. Fujimori, and Y. Tokura, *Rev. Mod. Phys.* **70**, 1039 (1998).  
[13] D. I. Khomskii, *Transition Metal Compounds* (Cambridge University Press, Cambridge, 2014).  
[14] M. Itoh, M. Tsuchiya, H. Tanaka, and K. Motoya, *J. Phys. Soc. Jpn.* **68**, 2783 (1999).  
[15] J. Akimitsu, H. Ichikawa, N. Eguchi, T. Miyano, M. Nishi, and K. Kakurai, *J. Phys. Soc. Jpn.* **70**, 3475 (2001).  
[16] H. Ichikawa, J. Akimitsu, M. Nishi, and K. Kakurai, *Physica B (Amsterdam, Neth.)* **281-282**, 482 (2000).  
[17] M. Ito, N. Tuji, F. Itoh, H. Adachi, E. Arakawa, K. Namikawa, H. Nakao, Y. Murakami, Y. Taguchi, and Y. Tokura, *J. Phys. Chem. Sol.* **65**, 1993 (2004).  
[18] I. A. Kibalin, Z. Yan, A. B. Voufack, S. Gueddida, B. Gillon, A. Gukasov, F. Porcher, A. M. Bataille, F. Morini, N. Clauser *et al.*, *Phys. Rev. B* **96**, 054426 (2017).  
[19] H. Nakao, Y. Wakabayashi, T. Kiyama, Y. Murakami, M. v. Zimmermann, J. P. Hill, D. Gibbs, S. Ishihara, Y. Taguchi, and Y. Tokura, *Phys. Rev. B* **66**, 184419 (2002).  
[20] F. Iga, M. Tsubota, M. Sawada, H. B. Huang, S. Kura, M. Takemura, K. Yaji, M. Nagira, A. Kimura, T. Jo, T. Takabatake, H. Namatame, and M. Taniguchi, *Phys. Rev. Lett.* **93**, 257207 (2004).  
[21] G. Khaliullin and S. Maekawa, *Phys. Rev. Lett.* **85**, 3950 (2000).  
[22] M. Cwik, T. Lorenz, J. Baier, R. Müller, G. André, F. Bourée, F. Lichtenberg, A. Freimuth, R. Schmitz, E. Müller-Hartmann, and M. Braden, *Phys. Rev. B* **68**, 060401(R) (2003).  
[23] M. W. Haverkort, Z. Hu, A. Tanaka, G. Ghiringhelli, H. Roth, M. Cwik, T. Lorenz, C. Schüßler-Langeheine, S. V. Streltsov, A. S. Mylnikova, V. I. Anisimov, C. de Nadai, N. B. Brookes, H. H. Hsieh, H.-J. Lin, C. T. Chen, T. Mizokawa, Y. Taguchi, Y. Tokura, D. I. Khomskii, and L. H. Tjeng, *Phys. Rev. Lett.* **94**, 056401 (2005).  
[24] T. Kiyama and M. Itoh, *Phys. Rev. Lett.* **91**, 167202 (2003).  
[25] M. Mochizuki and M. Imada, *Phys. Rev. Lett.* **91**, 167203 (2003).  
[26] P. Lunkenheimer, T. Rudolf, J. Hemberger, A. Pimenov, S. Tachos, F. Lichtenberg, and A. Loidl, *Phys. Rev. B* **68**, 245108 (2003).  
[27] M. Mochizuki and M. Imada, *J. Phys. Soc. Jpn.* **70**, 1777 (2001); **70**, 2872 (2001).  
[28] M. Mochizuki and M. Imada, *J. Phys. Soc. Jpn.* **73**, 1833 (2004).  
[29] P. Blaha, K. Schwarz, P. Sorantin, and S. Trickey, *Comput. Phys. Commun.* **59**, 399 (1990).  
[30] N. Marzari and D. Vanderbilt, *Phys. Rev. B* **56**, 12847 (1997).  
[31] T. Mizokawa and A. Fujimori, *Phys. Rev. B* **54**, 5368 (1996).  
[32] E. Gull, A. J. Millis, A. I. Lichtenstein, A. N. Rubtsov, M. Troyer, and P. Werner, *Rev. Mod. Phys.* **83**, 349 (2011).

- [33] D. A. Maclean, H.-N. Ng, and J. E. Greedan, *J. Solid State Chem.* **30**, 35 (1979).
- [34] Note that in Refs. [15, 16, 17, 18, 20] the local  $\mathbf{z}$  axis is in the direction of the longest Ti-O bond. This differs from the convention adopted in this work (see caption of Fig. 1).
- [35] M. Mochizuki and M. Imada, *New J. Phys.* **6**, 154 (2004).
- [36] A. M. Oleś, G. Khaliullin, P. Horsch, and L. F. Feiner, *Phys. Rev. B* **72**, 214431 (2005).
- [37] A. M. Oleś, in *The Physics of Correlated Insulators, Metals, and Superconductors*, edited by E. Pavarini, E. Koch, R. Scalettar, and R. M. Martin, Modeling and Simulation Vol. 7 (Verlag des Forschungszentrum Jülich, Jülich, 2017), p 5.1; *Acta Phys. Pol. A* **118**, 212 (2010).
- [38] A. B. Harris, T. Yildirim, A. Aharony, O. Entin-Wohlman, and I. Ya. Korenblit, *Phys. Rev. Lett.* **91**, 087206 (2003); *Phys. Rev. B* **69**, 035107 (2004).
- [39] M. Mochizuki and M. Imada, *J. Phys. Soc. Jpn.* **69**, 1982 (2000).